Title

Validation of vessel size imaging (VSI) in high-grade human gliomas using magnetic resonance imaging, image-guided biopsies, and quantitative immunohistochemistry

Journal

Scientific Reports, 9(1)

ISSN

2045-2322

Authors

Chakhoyan, Ararat

Yao, Jingwen

Leu, Kevin

et al.

Publication Date

2019

DOI

10.1038/s41598-018-37564-w

Peer reviewed

SCIENTIFIC REPORTS

OPEN

Validation of vessel size imaging (VSI) in high-grade human gliomas using magnetic resonance imaging, image-guided biopsies, and quantitative immunohistochemistry

Received: 20 July 2018
Accepted: 4 December 2018
Published online: 26 February 2019

Ararat Chakhoyan[1,2], Jingwen Yao[1,2,3], Kevin Leu[1,2], Whitney B. Pope[2], Noriko Salamon[2], William Yong[4], Albert Lai[5], Phioanh L. Nghiemphu[5], Richard G. Everson[6], Robert M. Prins[6], Linda M. Liau[6], David A. Nathanson[7], Timothy F. Cloughesy[5] & Benjamin M. Ellingson[1,2,3,8]

To evaluate the association between a vessel size index (VSI_{MRI}) derived from dynamic susceptibility contrast (DSC) perfusion imaging using a custom spin-and-gradient echo echoplanar imaging (SAGE-EPI) sequence and quantitative estimates of vessel morphometry based on immunohistochemistry from image-guided biopsy samples. The current study evaluated both relative cerebral blood volume (rCBV) and VSI_{MRI} in eleven patients with high-grade glioma (7 WHO grade III and 4 WHO grade IV). Following 26 MRI-guided glioma biopsies in these 11 patients, we evaluated tissue morphometry, including vessel density and average radius, using an automated procedure based on the endothelial cell marker CD31 to highlight tumor vasculature. Measures of rCBV and VSI_{MRI} were then compared to histological measures. We demonstrate good agreement between VSI measured by MRI and histology; $VSI_{MRI} = 13.67\,\mu m$ and $VSI_{Histology} = 12.60\,\mu m$, with slight overestimation of VSI_{MRI} in grade III patients compared to histology. rCBV showed a moderate but significant correlation with vessel density ($r = 0.42$, $p = 0.03$), and a correlation was also observed between VSI_{MRI} and $VSI_{Histology}$ ($r = 0.49$, $p = 0.01$). The current study supports the hypothesis that vessel size measures using MRI accurately reflect vessel caliber within high-grade gliomas, while traditional measures of rCBV are correlated with vessel density and not vessel caliber.

Neovascularization in gliomas plays an important role in response to anti-tumor strategies[1,2]. Various signaling pathways regulate this complex mechanism, including vascular co-option, angiogenesis, vascular mimicry, and endothelial cell trans-differentiation[3,4]. It is known that this tumor vasculature is functionally and morphologically abnormal[5]. The quantification of abnormal vessels on histology is a standard indicator of poor outcome for

[1]UCLA Brain Tumor Imaging Laboratory (BTIL), Center for Computer Vision and Imaging Biomarkers, David Geffen School of Medicine, University of California Los Angeles, Los Angeles, CA, USA. [2]Department of Radiological Sciences, David Geffen School of Medicine, University of California Los Angeles, Los Angeles, CA, USA. [3]Department of Bioengineering, Henry Samueli School of Engineering and Applied Science, University of California Los Angeles, Los Angeles, CA, USA. [4]Division of Neuropathology, Department of Pathology and Laboratory Medicine, David Geffen School of Medicine, University of California Los Angeles, Los Angeles, CA, USA. [5]Department of Neurology, Ronald Reagan UCLA Medical Center, University of California Los Angeles, Los Angeles, CA, USA. [6]Department of Neurosurgery, Ronald Reagan UCLA Medical Center, University of California Los Angeles, Los Angeles, CA, USA. [7]Department of Molecular and Medical Pharmacology, David Geffen UCLA School of Medicine, Los Angeles, CA, USA. [8]UCLA Neuro Oncology Program, David Geffen School of Medicine, University of California Los Angeles, Los Angeles, CA, USA. Correspondence and requests for materials should be addressed to B.M.E. (email: bellingson@mednet.ucla.edu)

glioma patients[6–8]. Using magnetic resonance imaging (MRI), several methods have been proposed that yield physiologic information about tumor vasculature, including blood flow and volume[9,10]. Theoretical Monte-Carlo simulations have suggested that T_2- and T_2*-weighted images acquired during dynamic susceptibility contrast (DSC) perfusion imaging are sensitive to microvasculature and larger vessels, respectively[11,12], by exploiting the differences in transverse relaxation rates R_2* and R_2 during the passage of contrast bolus through the vasculature[13]. This effect observed in small vessels is related to the magnitude of water diffusion, which is equivalent to the local susceptibility gradient. When the vascular bed is quantified with spin-echo (SE) sequence, the blood flow and volume are capillary weighted with a radius lower than 10 μm[13], while with gradient-echo (GE) sequence, the hemodynamic parameters are weighted to total vessels of all size[14]. In this way, separate or simultaneous acquisitions of SE and GE parameters have been speculated to be useful in more functional information of blood vessels architecture and its oxygenation[15–18]. For example, the ratio of peak ΔR_2*/ΔR_2 has been shown to correlate with histologically derived measures of vessel size in a preclinical C6 glioma xenograft model[14]. This promising preliminary evidence suggesting a close link between the average vessel size index derived from MRI (VSI_{MRI}) and histology ($VSI_{Histology}$) using preclinical models[16,19].

A separate model for estimating vessel size was established by Kiselev *et al.*[17,20] and incorporates measures of both cerebral blood volume and water diffusivity. In this model, the proportionality constant to scale differences between MRI and histology has not been thoroughly validated[17]. Additionally, in the previous publications, the normalized rCBV was set generically to 6%, which represents an extreme physiological conditions[21]. Recently, a single study involving glioma patients confirmed the association between this model and vascular morphometry using CD34 endothelial cell marker expression[22]; however, despite the high number of patients and biopsy samples in each individual patient, this study reported very few identifiable vessels (~10 per sample) in some glioma patients, likely related to the small biopsy size (1–1.5 mm in diameter).

In this current work, we quantified relative cerebral blood volume (rCBV) and VSI_{MRI} using a spin-and-gradient echo echoplanar imaging (SAGE-EPI) sequence during DSC perfusion MRI in patients with high-grade gliomas. The correlation between VSI_{MRI} and rCBV with vessel density and caliber from image-guided biopsies were examined after staining with endothelial cell marker, CD31, chosen as a specific marker of undifferentiated and differentiated microvasculature[23,24]. We hypothesized that Kiselev's model, which provide several corrections (both diffusion and perfusion components) to estimate vessel size, would be strongly associated with $VSI_{Histology}$.

Results

Typical example of T2w-FLAIR, post-contrast T1w, ADC, rCBV, VSI images as well as CD31 staining of high-grade glioma patients are shown in Fig. 1. The first patient, bearing an anaplastic oligodendroglioma lesion in the left frontal lobe, illustrated a lesion with hyperintensities on T2w-FLAIR images, increased ADC and rCBV as compared to corresponding NAWM (Fig. 1, upper). In contrast, VSI_{MRI} maps showed potential hyper-dense and large vessels in the edges of the lesion as demonstrated with targets overlaid on VSI maps (rectangles) and confirmed with CD31 staining. Patient B, harbored a glioblastoma in left parietal lobe (Fig. 1, bottom). This patient has a heterogeneous ring-enhancing lesion with perilesional edema, elevated ADC within the area of edema, increased rCBV in the posterior part of the tumor with increased and spatially heterogeneous measures of VSI_{MRI}. As confirmed with MRI and histology, high-grade gliomas patients demonstrate intra-tumoral vascular heterogeneity (CD31 staining) as highlighted by different targets from each patient.

We next assessed for each biopsy region, histological and MRI-derived features. From three-dimensional, 5 mm radius biopsy targets, we found a median number of vessel of 90 [interquartile range = 64.6–117.7], a median density of 40.6 per mm^2 [interquartile range = 29.8–78.6 per mm^2] and a median vessel diameter of 12.6 [interquartile range = 10.5–14.1 μm]. A median ADC of 1.30 μm^2/ms [interquartile range = 1.05–1.63 μm^2/ms] was measured within 5 mm biopsy targets, with a median rCBV of 1.39 [interquartile range = 1.00–2.36] and a median VSI of 13.6 μm^2 [interquartile range = 11.98–15.06 μm^2/ms].

Bland-Altman plot (Fig. 2A) suggests a significant difference between VSI measures between MRI and histology. Mean difference between MRI and histology was −1.13 μm (p = 0.03, Student's t-test) with 1.96 standard deviation values of the differences ranged from −0.41 μm to −2.22 μm for respectively, upper and lower limits. Black arrows in Fig. 2 indicate biopsy targets in WHO III gliomas where VSI_{MRI} overestimated vessel caliber compared with histology.

When directly comparing MR-based perfusion measures with histology (Fig. 3A–D), MRI-derived rCBV showed a moderate, but statistically significant correlation with histology-derived estimates of vessel density (r = 0.42, p = 0.032, Fig. 3A), but not with vessel caliber (r = −0.03, p = 0.874, Fig. 3B). Consistent with our original hypotheses, VSI_{MRI} was significantly correlated with vessel caliber (r = 0.49, p = 0.010, Fig. 3D), but was not correlated with vessel density obtained from histology (r = −0.01, p = 0.942, Fig. 3C).

Discussion

The current study supports the hypothesis that VSI measured using MRI is highly correlated with the actual vessel caliber in underlying tumor tissue within high-grade gliomas. Additionally, the current study also supports the notion that rCBV measures from MRI correlated with vessel density within the tumor.

There have been several MRI based studies demonstrated the feasibility of VSI or similar measurements. While early studies by Donahue *et al.*[25] and Schmainda *et al.*[26] have demonstrated the clinical feasibility of measures of mean vessel diameter (mVD), VSI measures that take into account both rCBV and ADC, which can influence vessel size measurements, have only been thoroughly evaluated orthotopic brain tumor models, which found with good quantitative agreement of histology[19,27]. However, all these studies have used high field MRI (up to 4.7 T) with potential imperfections of main B_0 and transmit B_1 magnetic fields, which should be considered[28] for the appropriate quantification ΔR_2*, ΔR_2 and finally VSI. A recent publication using Tropès model showed that,

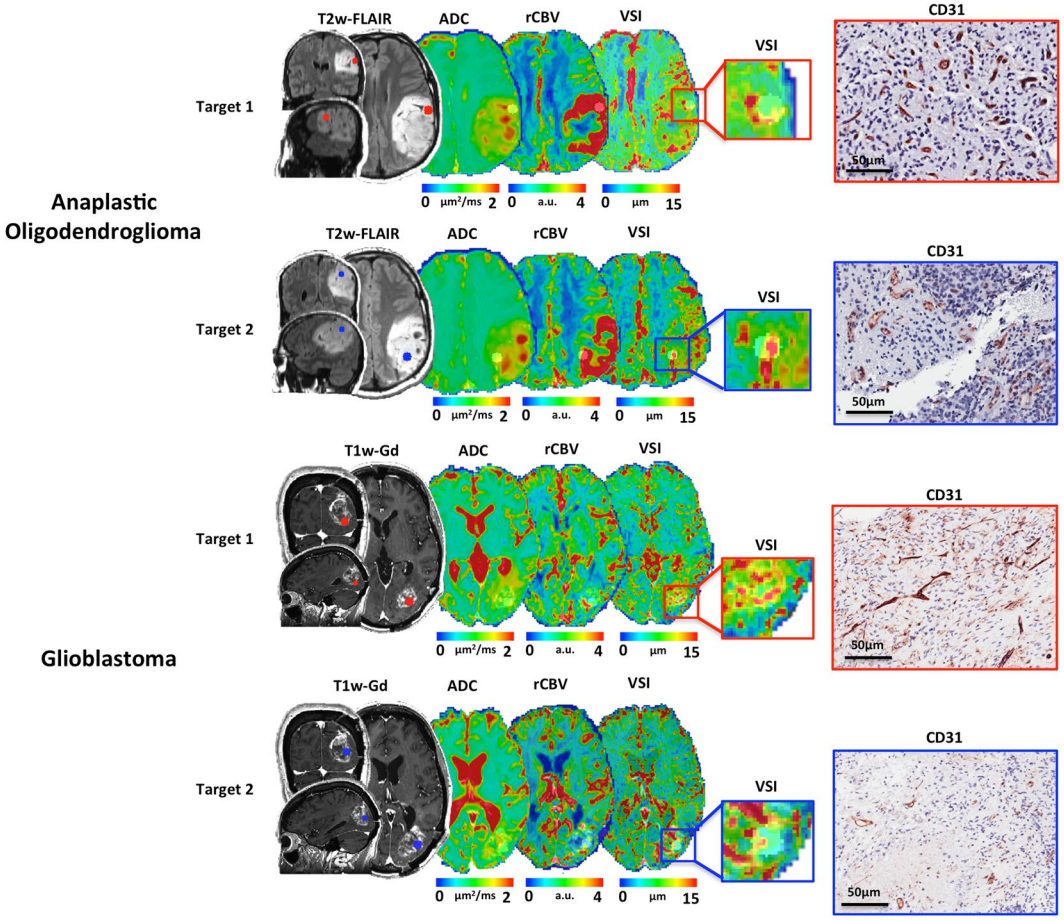

Figure 1. Two representative high-grade glioma patients are reported with their respective biopsy targets. T2w-FLAIR (upper) or post-contrast T1w (bottom) images were used for anatomical reference in tissue sampling in various tumor grades. ADC, rCBV and VSI_{MRI} maps are shown for each patient. The first patient (upper) has a WHO grade III, Anaplastic Oligodendroglioma. The brain lesion is located in the left frontal lobe. The second patient (bottom) is a WHO Grade IV glioblastoma with a brain lesion located in the left parietal lobe. An elevated ADC and rCBV showed in both patients within tumor areas. Glioblastoma patient show an increased heterogeneity of vessel size within and around enhancing areas. Examples of tissue slides with stained CD31 positive vessels for each representative target. As observed with VSI_{MRI}, in both grade III and IV, CD31 positive vessels are present with spatial heterogeneity in terms of density and morphometry.

with high-field MRI (7 T), VSI measurements tend to overestimate as compared to two-photon laser scanning microscopy[29]. This observation may be due to underestimation of blood volume in the tumor and/or heterogeneous distribution of vessel radii.

Recently, the Kiselev model VSI_{MRI} has been reported with adjusted rCBV values for healthy tissue to more typical values for blood volume (3.2%)[22]. The former study also compared histological findings (vessel diameter) with MRI results (rCBV and VSI). With an averaged rCBV of 5.99% (uncorrected for contrast leakage); an ADC of 1.02 μm/ms, authors reported an average VSI of 67.13 μm in high-grade glioma, which is two times higher than what they reported for mean vessel diameter (31 μm) but has good agreement with maximum vessel diameter (69.8 μm). However, the tissue targeting protocol of that study may be biased, as for 4 glioblastoma patients, authors reported less than 6 detected vessels with CD34 endothelial marker. This marker is known to be specific for differentiated, well-formed vessels (including normal vessels)[30] which makes results difficult to interpret.

With the same range of healthy tissue blood volume, 3%, Xu *et al.*[31], reported an average VSI of 13.8 μm in gray matter and 13.1 μm in white matter. These results of healthy tissues are correlates well with vessel radius values reported by Christen *et al.*[30], (12.6 ± 2.4 μm with 3.1% of CBV in gray matter). Note that in our study, the rCBV is only normalized to contralateral NAWM and the average rCBV was 0.96, which in turns, results to an average VSI_{MRI} of normal appearing brain 4.51 μm (results not shown). Additionally, a study of confocal laser microscopy reports an average vessel diameter of human cortex lower than MRI approaches; 7.82 ± 3.52 μm[31], which is in accord to other mammalian neocortex vascular diameter (e.g. cat and rat; ranged from 4.2 to 7 μm), reviewed by Pawlik *et al.*[32]. Indeed, the fact that VSI_{MRI} correlates to $VSI_{Histology}$ independently of vessel density is very promising; however, some overestimation is reported in our current study, especially in the WHO grade III patients and in preclinical studies[15,16]. This overestimation from VSI_{MRI} is consistent with results of Kellner *et al.*[22],

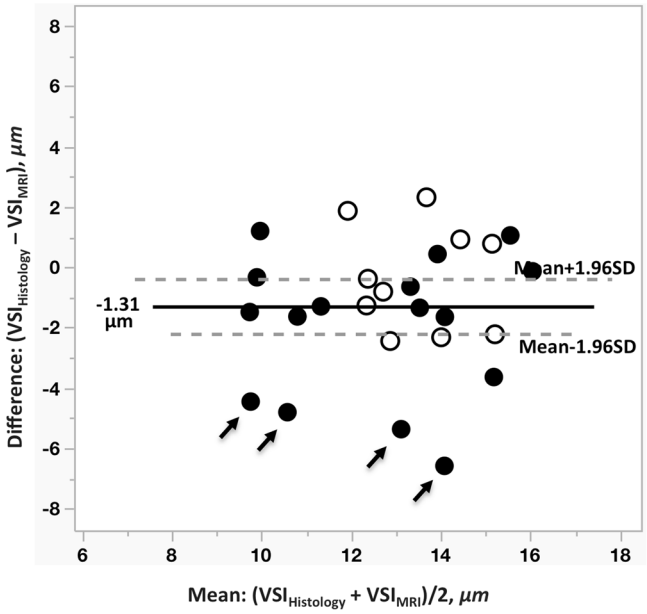

Figure 2. Bland-Altman plot represents potential bias of agreement between these two techniques. A number of points display higher difference between VSI_{MRI} and $VSI_{Histology}$, especially in grade III (black arrows). Filled and unfilled circles presenting targets from grade III and grade IV, respectively.

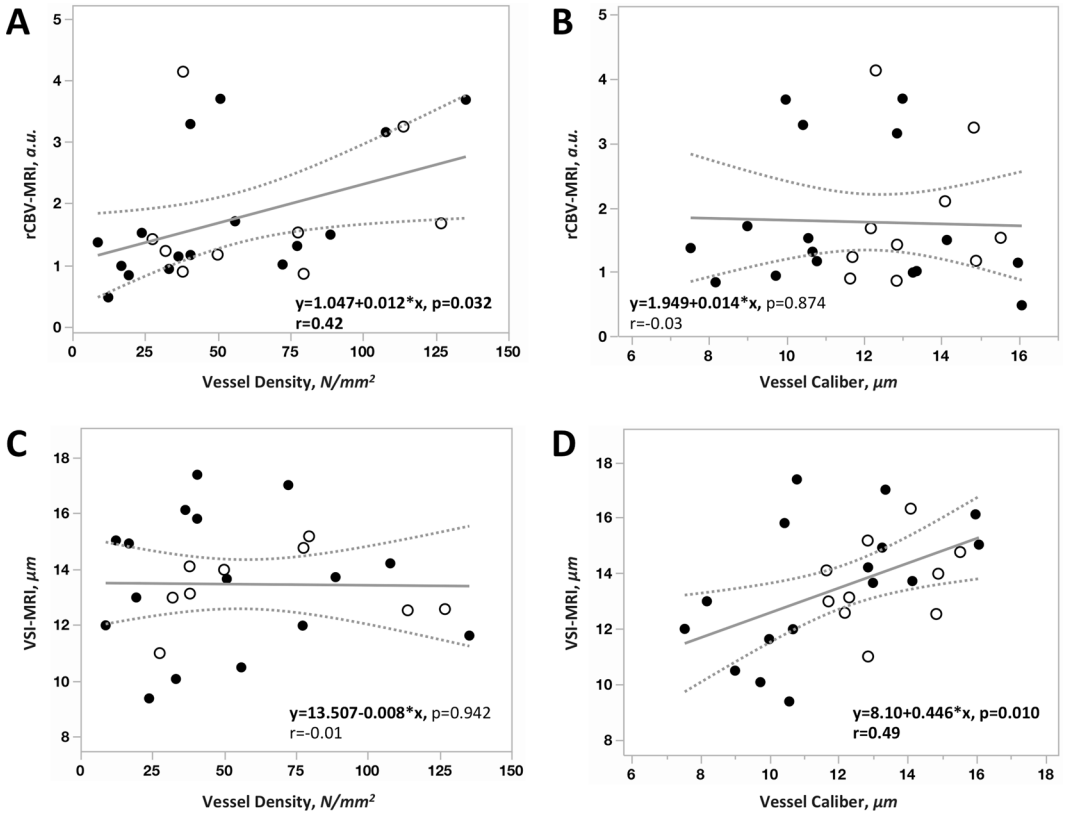

Figure 3. Linear correlation was performed between rCBV, VSI_{MRI} and their corresponding histology value; vessel density and vessel caliber ($VSI_{Histology}$). Positive linear correlation was found between rCBV vs. vessel density (**A**, $r = 0.42$, $p = 0.032$) as well as between VSI_{MRI} and vessel caliber (**D**, $r = 0.49$, $p = 0.010$). However, no direct relationship was observed between rCBV and vessel caliber (**B**). VSI_{MRI} measures are independent of vessel density (**C**). The filled and unfilled circles presenting targets from grade III and grade IV, respectively.

as well as from a rodent study[19], and occurs especially in small vessel sizes. The following imperfection could be overcome by assessing VSI_{MRI} with more flexible topological models including vessel length, radius, and vessel orientation angles[33]. Additionally, our observations regarding the association between rCBV and vessel density appear consistent with previously reported results from tumor bulk[34]; however, tumor vessel size heterogeneity often influences the reliability of rCBV estimates in comparison with histology[35].

There were certain limitations of our experimental setup that should be addressed. First, the limited spatial resolution and the registration of lower-resolution SAGE-EPI to high-resolution 3D-T1w images may have resulted in potential bias. It is important to note that precise targeting of brain tissue during biopsy is a significant technical challenge, as inherent changes in the brain position during craniotomy may occur, which could directly affect accurate MRI-guided sampling of tumor specimens. Additionally, the use of rCBV as a normalized approximation of rCBV is another limitation of VSI modeling which could have led to inaccuracies. Also, the specificity of VSI_{MRI} to perfused vessels can also result in discordance between VSI measurements and histology. Moreover, the "delta" term that describes the residual signal differences from imperfectly matched slice profiles may vary over time and may be dependent on the radiofrequency architecture and other details. However, this did not vary more than 3–6% across patients over time in our study (results not shown), so it likely did not influence our results. Finally, contrast-to-noise (CNR) ratio over time may have been affected by use of a single dose of contrast agent, particularly for estimation of R_2, so this should also be recognized.

In summary, the current study estimated VSI with SAGE-EPI in high-grade glioma patients and correlated this measurement with histological characteristics of the vessel architecture. Results demonstrated that VSI measured with MRI is correlated with vascular caliber, while vessel density is mostly linked to measures of rCBV.

Material and Methods

Patients. This study was performed in accordance with the Health Insurance Portability and Accountability Act (HIPAA), and all patients provided signed, informed written consent for all experimental protocols used in the current, institutional review board approved study (UCLA Medical IRB 2, #14-001261). Eleven patients with histologically confirmed high-grade glioma (7 WHO grade III [4 *de novo* and 3 at first recurrence] and 4 WHO grade IV glioblastoma [2 *de novo* and 2 at first recurrence]) have been enrolled in this retrospective study. From 4 *de novo* grade III patients, 3 were anaplastic oligodendroglioma and one diffuse astrocytoma (IDH mutant). From remaining 3 recurrent grade III patients, 2 were anaplastic gangliogliomas and one anaplastic astrocytoma. For 5 enrolled recurrent patients, 4 received standard craniotomy, followed by chemoradiation prior to the second craniotomy. One anaplastic oligodendroglioma received only craniotomy in 2009 and image-guided biopsy was performed in 2015. Of the 11 enrolled patients (9 men and 2 woman), the median age was 50.8 years ranged from 28.5 to 67.9 years. Both MRI and neuropathology specimens were obtained and analyzed with respect to local ethical committee approval. In total, 26 MRI-based targets were biopsied and analyzed.

Magnetic Resonance Imaging. All MRI images were acquired using a 3 Tesla MRI system (Siemens; Erlangen, Germany) in compliance with the international standardized brain tumor imaging protocol (BTIP)[36]. Briefly, 1 mm isotropic, 3D MPRAGE T1-weighted images were acquired prior to contrast injection, along with axial T2-weighted images and T2-weighted fluid attenuation inversion recovery (FLAIR) images. Axial diffusion-weighted imaging (DWI) was performed using a single-shot echo-planar imaging with three b values (0, 500 and 1000 sec/mm^2) to compute the apparent diffusion coefficient (ADC). T_2-, T_2-weighted FLAIR, and DWI were all collected with 3-mm slice thickness and no interslice gap.

VSI_{MRI} and rCBV were calculated by acquiring dynamic SAGE-EPI data during contrast injection. A pre-dose 0.025 mmol/kg of Gd-DTPA was first administrated reduce contrast extravasation, followed by a bolus dose of 0.075 mmol/kg. The SAGE-EPI readout consisted of two gradient echoes ($TE_1 = 14.0$ ms; $TE_2 = 34.1$ ms), an asymmetric spin echo ($TE_3 = 58.0$ ms) and a spin echo ($TE_4 = 92.4$ ms) EPI train with GRAPPA acceleration factor of 3. The repetition time was 2000 ms with a slice thickness of 5 mm and no additional spacing between slices. The resolution was set to 1.875×1.875 mm with a total matrix size of 240×218 mm. A total of 90 repetitions were obtained over 19 axial slices. Following DSC perfusion acquisition, a parameter matched, 1-mm isotropic, post-contrast 3D MPRAGE T1-weighted dataset was acquired according to BTIP.

MRI post-processing. Dynamic susceptibility contrast based relative cerebral blood volume (rCBV) maps were calculated using an in-house bi-directional contrast agent leakage correction algorithm that accounts for both contrast flux out of and into the vasculature[37]. Normalization of rCBV maps was performed by comparison to contralateral normal appearing white matter (NAWM).

Estimation of VSI_{MRI} was based on the Kiselev model[17], which is built upon on the basis of Tropès model[15] with additional consideration for rCBV values and use the ratio of $\Delta R_2^*/\Delta R_2$ as a result of average vessel size index, expressed in μm:

$$VSI_{\mu m} = 0.867(rCBV \cdot ADC)^{1/2}\left(\frac{\Delta \mathbf{R}_2^*}{\Delta R_2^{3/2}}\right) \quad (1)$$

where ΔR_2^* and ΔR_2 represents the maximum changes in the transverse relaxation rates obtained from solving the following linear equation[38]:

$$A = Y^{-1}S \quad (2)$$

where

$$S = \begin{pmatrix} \ln(S_1) \\ \ln(S_2) \\ \ln(S_3) \\ \ln(S_4) \end{pmatrix}, \mathbf{Y} = \begin{pmatrix} 1 & 0 & -TE_1 & 0 \\ 1 & 0 & -TE_2 & 0 \\ 1 & -1 & -TE_4 + TE_3 & TE_4 - 2 \cdot TE_3 \\ 1 & -1 & 0 & -TE_4 \end{pmatrix}, \mathbf{A} = \begin{pmatrix} \ln(S_0) \\ \ln(\delta) \\ R_2^* \\ R_2 \end{pmatrix} \quad (3)$$

where S_n is signal magnitude for the n^{th} echo and δ is the differences in residual signal differences introduced from imperfectly matched slice profiles. Those discordances are related to the echo trains, before and after refocusing pulse[39].

Image registration. All images (T2w, FLAIR, ADC, rCBV, and VSI_{MRI}) were registered to 1-mm isotropic post-contrast T1-weighted images using a 12-degree-of-freedom, automated linear registration tool using a correlation ratio cost function (FSL-FLIRT, http://www.fmrib.ox.ac.uk/fsl/). All registered maps were visually inspected and, if necessary, manually corrected in the event of misregistration.

Image-guided biopsy and Immunohistochemistry. After image acquisition, one to three (5 mm radius) targets were identified on post-contrast T1w and/or fused T2w-FLAIR images within contrast-enhancing (tumor core) and non-enhancing tumor regions, respectively. These targets were loaded into BrainLab Neuronavigation software (BrainLab AG, Munich, Germany). Following target identification, a critical review was performed by the primary neurosurgeon to make sure that targets were within the final resection volume, did not affect brain eloquent areas (assessed by blood level dependent contrast (BOLD) activation maps) and were not within the main trajectory of large white matter tracts (assessed by diffusion tensor imaging).

Following image-guided resection, biopsy samples were transferred to the Department of Pathology & Laboratory Medicine for immunohistochemistry (IHC) staining. IHC using an antibody against the endothelial cell marker CD31 has been chosen. Staining was performed on 4 μm paraffin-embedded sections after initial dewaxing with xylene and rehydration through graded ethanol, followed by antigen retrieval with a pH 6.0 Antigen Retrival Solution (Biocare Medical) in a Decloaking pressure cooker at 95 °C for 40 min. Tissue sections were then treated with 3% hydrogen peroxide (LOT 161509; Fisher Chemical) and with Background Sniper (Biocare Medical, Concord, CA, USA) to reduce nonspecific background staining. All slides were then incubated at room temperature for 80 min with ready to use primary antibody for CD31 (Biocare, 090215) followed by detection with the MACH 4 Mouse HRP- Polymer Detection kit (Biocare Medical). VECTOR NovaRED (SK-4800; Vector Laboratories, Inc.) was applied as chromogen.

Segmentation of blood vessels from CD31 staining and quantification of $VSI_{Histology}$. Segmentation of CD31 was performed on 2D stained slices based on the CAIMAN algorithm[40]. Briefly, the algorithm exploits the distinctive hues of stained vascular endothelial cells, cell nuclei and background. A region-growing algorithm using the seeds created with the previous step and a 3D Hue, Saturation, Value (HSV) color model. Three major morphological tasks were then performed: (1) joining separate objects that were likely to belong to a single vessel; (2) closing objects that had a narrow gap around their periphery; and (3) splitting objects with multiple lumens into individual vessels. A hole fill was performed to include vessel lumen in the calculation of vessel radius. Manual correction was performed on the stained slices with obvious errors. A total of 3 regions of interest were selected for each target and the average quantification of these 3 values was attributed to each target.

After segmentation, vessel density (number divided by the total area of the sample) was computed and expressed in N/mm^2. Quantification of $VSI_{Histology}$ on the stained slides were then performed following a previously described model[16] (assuming vessels are randomly oriented, continuous cylinders with different radii):

$$VSI_{histo} = \left(\frac{\sum_i n(r_i) . \ r_i^{4/3}}{\sum_i n(r_i) . \ r_i^2} \right)^{-3/2} \quad (4)$$

where $n(r_i)$ is the number of vessels with radius r. Final results are expressed in μm.

Statistical analyses. A nonparametric Wilcoxon-Mann-Whitney test was used to assess potential statistical differences in both WHO grade III and IV for all MRI and histology-derived parameters. Regression was performed to assess the degree of agreement between MRI (rCBV and VSI_{MRI}) and histology (density and $VSI_{Histology}$). An alternative analysis of potential bias determination between these two techniques (VSI_{MRI} vs. $VSI_{Histology}$) was performed using a Bland-Altman test. The difference between VSI_{MRI} vs. $VSI_{Histology}$ was assessed using Student's *t*-test, after checking the normality of each distribution using a Shapiro-Wilk test[41,42].

References

1. Jain, R. K. *et al.* Angiogenesis in brain tumours. *Nat. Rev. Neurosci.* **8**, 610–22 (2007).
2. Batchelor, T. T. *et al.* Improved tumor oxygenation and survival in glioblastoma patients who show increased blood perfusion after cediranib and chemoradiation. *Proc. Natl. Acad. Sci.* **110**, 19059–64 (2013).
3. Hardee, M. E. & Zagzag, D. Mechanisms of glioma-associated neovascularization. *Am. J. Pathol.* **181**, 1126–1141 (2012).
4. Das, S. & Marsden, P. A. Angiogenesis in Glioblastoma. *N. Engl. J. Med.* **369**, 1561–1563 (2013).
5. Mahase, S. *et al.* Hypoxia-mediated mechanisms associated with antiangiogenic treatment resistance in Glioblastomas. *Am. J. Pathol.* **187**, 940–953 (2017).
6. Emblem, K. E. *et al.* Glioma grading by using histogram analysis of blood volume heterogeneity from MR-derived cerebral blood volume maps. *Radiology.* **247**, 808–17 (2008).

7. Chen, W. *et al*. Overexpression of vascular endothelial growth factor indicates poor outcomes of glioma: a systematic review and meta-analysis. *Int. J. Clin. Exp. Med*. **8**, 8709–19 (2015).
8. Gerstner, E. *et al*. ACRIN 6684: Assessment of tumor hypoxia in newly diagnosed GBM using 18F-FMISO PET and MRI. *Clin. Cancer. Res.* **15**, 5079–5086 (2016).
9. Barbier, E. L., Lamalle, L. & Décorps, M. Methodology of Brain Perfusion Imaging. *J. Magn. Reson. Imaging.* **520**, 496–520 (2001).
10. Weber, M. A. *et al*. Perfusion measurement using the T2* contrast media dynamics in neuro-oncology. Physical basics and clinical applications. *Radiologe* **45**, 618–32 (2005).
11. Rosen, B. R. *et al*. Contrast agents and cerebral hemodynamics. *Magn. Reson. Med.* **19**, 285–92 (1991).
12. Pathak, A. P., Ward, B. D. & Schmainda, K. M. A novel technique for modeling susceptibility-based contrast mechanisms for arbitrary microvascular geometries: The finite perturber method. *Neuroimage* **40**, 1130–43 (2008).
13. Boxerman, J. L. *et al*. MR Contrast due to intravascular magnetic susceptibility perturbations. *Magn. Reson. Med.* **34**, 555–66 (1995).
14. Dennie, J. *et al*. NMR imaging of changes in vascular morphology due to tumor angiogenesis. *Magn. Reson. Med.* **40**, 793–9 (1998).
15. Troprès, I. *et al*. Vessel size imaging. *Magn. Reson. Med.* **45**, 397–408 (2001).
16. Troprès, I. *et al*. *In vivo* assessment of tumoral angiogenesis. *Magn. Reson. Med.* **51**, 533–41 (2004).
17. Kiselev, V. G. *et al*. Vessel size imaging in humans. *Magn. Reson. Med.* **53**, 553–63 (2005).
18. Steele, E. L. *et al*. Vessel calibre—a potential MRI biomarker of tumour response in clinical trials. *Nat. Rev. Clin. Oncol.* **11**, 566–84 (2014).
19. Valable, S. *et al*. Assessment of blood volume, vessel size, and the expression of angiogenic factors in two rat glioma models: a longitudinal *in vivo* and *ex vivo* study. *NMR Biomed.* **21**, 1043–56 (2008).
20. Xu, C. *et al*. Dynamic hysteresis between gradient echo and spin echo attenuations in dynamic susceptibility contrast imaging. *Magn. Reson. Med.* **69**, 981–91 (2013).
21. Østergaard, L. *et al*. Modeling cerebral blood flow and flow heterogeneity from magnetic resonance residue data. *J. Cereb. Blood. Flow. Metab.* **19**, 690–9 (1999).
22. Kellner, E. *et al*. MR evaluation of vessel size imaging of human gliomas: Validation by histopathology. *J. Magn. Reson. Imaging.* **42**, 1117–25 (2015).
23. Giatromanolaki, A. *et al*. Comparative evaluation of angiogenesis assessment with anti-gactor-Vill and anti-CD31 immunostaining in non-small cell lung cancer. *Clin. Cancer. Res.* **3**, 2485–92 (1997).
24. Caraffi, S. *et al*. Microcirculation density and maturity in uterine and soft tissue leiomyosarcomas: An immunohistochemical study. *Histol Histopathol.* **30**, 69–76 (2015).
25. Donahue, K. M. *et al*. Utility of simultaneously acquired gradient-echo and spin-echo cerebral blood volume and morphology maps in brain tumor patients. *Magn. Reson. Med.* **43**, 845–53 (2000).
26. Schmainda, K. M. *et al*. Characterization of a First-Pass Gradient-Echo Spin-Echo Method to Predict Brain Tumor Grade and Angiogenesis. *Am. J. Neuroradiol.* **25**, 1524–32 (2004).
27. Farrar, C. T. *et al*. *In vivo* validation of MRI vessel caliber index measurement methods with intravital optical microscopy in a U87 mouse brain tumor model. *Neuro Oncol.* **12**, 341–50 (2010).
28. Deoni, S. C. Correction of main and transmit magnetic field (B0 and B1) inhomogeneity effects in multicomponent-driven equilibrium single-pulse observation of T1 and T2. *Magn. Reson. Med.* **65**, 1021–35 (2011).
29. Douma, K. *et al*. Evaluation of magnetic resonance vessel size imaging by two-photon laser scanning microscopy. *Magn. Reson. Med.* **63**, 930–9 (2010).
30. Suster, S. & Wong, T. Y. On the discriminatory value of anti-HPCA-1 (CD-34) in the differential diagnosis of benign and malignant cutaneous vascular proliferations. *Am. J. Dermatopathol.* **16**, 355–63 (1994).
31. Lauwers, F. *et al*. Morphometry of the human cerebral cortex microcirculation: General characteristics and space-related profiles. *Neuroimage* **39**, 936–48 (2008).
32. Pawlik, G., Rackl, A. & Bing, R. J. Quantitative capillary topography and blood flow in the cerebral cortex of cats: an *in vivo* microscopic study. *Brain Res.* **208**, 35–58 (1981).
33. Shazeeb, M. S., Kalpathy-Cramer, J. & Issa, B. MRI simulation study investigating effects of vessel topology, diffusion, and susceptibility on transverse relaxation rates using a cylinder fork model. *Sci. Rep.* **14**(7), 16223 (2017).
34. Sadeghi, N. *et al*. Apparent diffusion coefficient and cerebral blood volume in brain gliomas: relation to tumor cell density and tumor microvessel density based on stereotactic biopsies. *Am. J. Neuroradiol.* **29**, 476–82 (2008).
35. Hu, L. S. *et al*. Correlations between perfusion MR imaging cerebral blood volume, microvessel quantification, and clinical outcome using stereotactic analysis in recurrent high-grade glioma. *Am. J. Neuroradiol.* **33**, 69–76 (2012).
36. Ellingson, B. M. *et al*. Consensus recommendations for a standardized Brain Tumor Imaging Protocol in clinical trials. *Neuro Oncol.* **17**, 1188–98 (2015).
37. Leu, K. *et al*. Bidirectional Contrast agent leakage correction of dynamic susceptibility contrast (DSC)-MRI improves cerebral blood volume estimation and survival prediction in recurrent glioblastoma treated with bevacizumab. *J. Magn. Reson. Imaging.* **44**, 1229–37 (2016).
38. Schmiedeskamp, H. *et al*. Combined spin- and gradient-echo perfusion-weighted imaging. *Magn. Reson. Med.* **68**, 30–40 (2012).
39. Schmiedeskamp, H., Straka, M. & Bammer, R. Compensation of slice profile mismatch in combined spin- and gradient-echo echo-planar imaging pulse sequences. *Magn. Reson. Med.* **67**, 378–88 (2012).
40. Reyes-Aldasoro, C. C. *et al*. An automatic algorithm for the segmentation and morphological analysis of microvessels in immunostained histological tumour sections. *J. Microsc.* **242**, 262–78 (2011).
41. Xu, C. *et al*. Vessel size imaging reveals pathological changes of microvessel density and size in acute ischemia. *J. Cereb. Blood. Flow. Metab.* **31**, 1687–95 (2011).
42. Christen, T. *et al*. MR Vascular Fingerprinting: A new approach to computecerebral blood volume, mean vessel radius, and oxygenation maps in the human brain. *Neuroimage* **89**, 262–270 (2014).

Acknowledgements

We thank Mitra D. Harati for helpful immunohistochemical staining. *Hoffman La-Roche; Siemens; Agios; Janssen* B.E. and K.L.; Patent: U.S. 62/211,852 – Multi-echo spin-, asymmetric spin-, and gradient-echo echo-planar imaging MRI pulse sequence. American Cancer Society (ACS) Research Scholar Grant (RSG-15-003-01-CCE) (Ellingson); Art of the Brain (Cloughesy); UCLA SPORE in Brain Cancer (NIH/NCI 1P50CA211015-01A1) (Ellingson, Liau, Nghiemphu, Lai, Pope, Cloughesy); NIH/NCI 1R21CA223757-01 (Ellingson).

Author Contributions

Study design: A.C. and B.E. Biopsy and immunohistochemistry: L.M.L., W.Y. Data analyses: A.C., J.Y., K.L., Sequence programming: K.L. Manuscript writing: A.C. and B.E. Manuscript Revision: W.B.P., N.S., A.L., P.L.N., R.G.E., R.P., D.A.N. and T.F.C. Approval of the final version: All authors.

Additional Information

Competing Interests: B.E.; Advisory Board – Hoffman La-Roche; Siemens; Nativis; Medicenna; MedQIA; Bristol Meyers Squibb; Imaging Endpoints; Agios. Paid Consultant – Nativis; MedQIA; Siemens; Hoffman La-Roche; Imaging Endpoints; Medicenna; Agios.

Publisher's note: Springer Nature remains neutral with regard to jurisdictional claims in published maps and institutional affiliations.